J|A|C|S
ARTICLES
Published on Web 05/03/2006

Triplet Energy Back Transfer in Conjugated Polymers with Pendant Phosphorescent Iridium Complexes

Nicholas R. Evans,[†] Lekshmi Sudha Devi,[‡] Chris S. K. Mak,[†] Scott E. Watkins,[†,§] Sofia I. Pascu,[†] Anna Köhler,[‡,||] Richard H. Friend,[‡] Charlotte K. Williams,[†,⊥] and Andrew B. Holmes*[,§,⊥]

Contribution from Melville Laboratory for Polymer Synthesis, Department of Chemistry, University of Cambridge, Lensfield Road, Cambridge CB2 1EW, United Kingdom, Cavendish Laboratory, Department of Physics, University of Cambridge, Madingley Road, Cambridge CB3 0HE, United Kingdom, School of Chemistry, University of Melbourne, Victoria 3010, Australia, Institute of Physics, University of Potsdam, Am Neuen Palais, Potsdam 14469, Germany, and Department of Chemistry, Imperial College, South Kensington, London, SW7 2AZ, United Kingdom

Received December 12, 2005; E-mail: aholmes@unimelb.edu.au

Abstract: The nature of Dexter triplet energy transfer between bonded systems of a red phosphorescent iridium complex **13** and a conjugated polymer, polyfluorene, has been investigated in electrophosphorescent organic light-emitting diodes. Red-emitting phosphorescent iridium complexes based on the $[Ir(btp)_2(acac)]$ fragment (where btp is 2-(2′-benzo[*b*]thienyl)pyridinato and acac is acetylacetonate) have been attached either directly (spacerless) or through a $-(CH_2)_8-$ chain (octamethylene-tethered) at the 9-position of a 9-octylfluorene host. The resulting dibromo-functionalized spacerless (**8**) or octamethylene-tethered (**12**) fluorene monomers were chain extended by Suzuki polycondensations using the bis(boronate)-terminated fluorene macromonomers **16** in the presence of end-capping chlorobenzene solvent to produce the statistical spacerless (**17**) and octamethylene-tethered (**18**) copolymers containing an even dispersion of the pendant phosphorescent fragments. The spacerless monomer **12** adopts a face-to-face conformation with a separation of only 3.6 Å between the iridium complex and fluorenyl group, as shown by X-ray analysis of a single crystal, and this facilitates intramolecular triplet energy transfer in the spacerless copolymers **17**. The photo- and electroluminescence efficiencies of the octamethylene-tethered copolymers **18** are double those of the spacerless copolymers **17**, and this is consistent with suppression of the back transfer of triplets from the red phosphorescent iridium complex to the polyfluorene backbone in **18**. The incorporation of a $-(CH_2)_8-$ chain between the polymer host and phosphorescent guest is thus an important design principle for achieving higher efficiencies in those electrophosphorescent organic light-emitting diodes for which the triplet energy levels of the host and guest are similar.

Introduction

The discovery of electroluminescence from small molecules[1] and conjugated polymers[2] has stimulated intense interest in the field of organic light-emitting diodes (OLEDs). In an OLED, visible light is generated through the radiative decay of excitons (excited states).[1,2] Excitons having either a singlet or triplet spin state arise from the recombination of charges within thin organic layers sandwiched between opposing electrodes under the application of bias voltage.[3] Models of spin statistics predict that the electron−hole recombination event should produce three times as many triplets as singlets,[4] and this has been confirmed experimentally for electroluminescent devices fabricated from small molecules.[5] For polymers, there are reports of the singlet-to-triplet ratio ranging from 1:1[6] to 1:3.[7,8] The singlet−triplet ratio is of interest because the radiative decay of triplet excitons to the singlet ground state is formally forbidden by a requirement for spin conservation.[9] The emissive layers of the earliest OLEDs were composed of fluorescent polymers[10] and/or small molecules, in which only the singlet excitons could decay

[†] Melville Laboratory for Polymer Synthesis, University of Cambridge.
[‡] Cavendish Laboratory, University of Cambridge.
[§] School of Chemistry, University of Melbourne.
[||] Institute of Physics, University of Potsdam.
[⊥] Department of Chemistry, Imperial College.

(1) Tang, C. W.; VanSlyke, S. A. *Appl. Phys. Lett.* **1987**, *51*, 913−915.
(2) Burroughes, J. H.; Bradley, D. D. C.; Brown, A. R.; Marks, R. N.; Mackay, K.; Friend, R. H.; Burn, P. L.; Holmes, A. B. *Nature* **1990**, *347*, 539−541.
(3) Brown, A. R.; Bradley, D. D. C.; Burroughes, J. H.; Friend, R. H.; Greenham, N. C.; Burn, P. L.; Holmes, A. B.; Kraft, A. *Appl. Phys. Lett.* **1992**, *61*, 2793−2795.
(4) For reviews, see: (a) Köhler, A.; Wilson, J. S.; Friend, R. H. *Adv. Mater.* **2002**, *14*, 701−707. (b) Wohlgenannt, M.; Vardeny, Z. V. *J. Phys.: Condens. Matter* **2003**, *15*, R83−R107. (c) Köhler, A.; Wilson, J. *Org. Electron.* **2003**, *4*, 179−189.
(5) Baldo, M. A.; O'Brien, D. F.; Thompson, M. E.; Forrest, S. R. *Phys. Rev. B* **1999**, *60*, 14422−14428.
(6) Wilson, J. S.; Dhoot, A. S.; Seeley, A. J. A. B.; Khan, M. S.; Köhler, A.; Friend, R. H. *Nature* **2001**, *413*, 828−831.
(7) Segal, M.; Baldo, M. A.; Holmes, R. J.; Forrest, S. R.; Soos, Z. G. *Phys. Rev. B: Condens. Matter* **2003**, *68*, 075211.
(8) Reufer, M.; Walter, M. J.; Lagoudakis, P. G.; Hummel, A. B.; Kolb, J. S.; Roskos, H. G.; Scherf, U.; Lupton, J. M. *Nat. Mater.* **2005**, *4*, 340−346.
(9) Turro, N. J. *Modern Molecular Photochemistry*; Benjamin/Cummings Publishing: Menlo Park, CA, 1978.

radiatively.[1,2] A significant step in the development of highly efficient OLEDs was the addition of phosphorescent dopants to these layers in order to harvest both the singlet and triplet excitons as light.[11−14] This innovation has led to near quantitative internal efficiencies in OLEDs that are based on organic small molecules.[15] Although the emissive layer of a conjugated-polymer OLED can also be doped with phosphorescent guest molecules,[16,17] issues such as triplet energy confinement and phase separation must be addressed as is described below.

The electronic energy levels of conjugated polymers are stabilized by the π-bonding delocalized along the chain.[18] Hence conjugated polymers often exhibit relatively low triplet energy levels, unless the extent of conjugation has been limited by design.[19,20] For efficient electrophosphorescence to occur in a doped OLED, the triplet energy level of the phosphorescent guest should be below that of the conjugated polymer host.[16,21] This is in order to inhibit migration of excitons from the guest to the nonphosphorescent host by Dexter triplet energy transfer. The triplet energy level in members of the blue fluorescent polyfluorene family of conjugated polymers is found at ca. 2.1 eV,[22] which limits the use of polyfluorenes in electrophosphorescent OLEDs to that of host for red phosphorescent guests (triplet energy level of below 2.1 eV),[16,23,24] the subject matter of the present study.

The emissive layers in electrophosphorescent small-molecule OLEDs are prepared by simultaneous vacuum deposition of both phosphorescent guest and fluorescent host molecules, and phase separation is not an issue.[12,15] In contrast, a blend of polymer and phosphorescent guest is typically deposited from solution by spin-coating or ink-jet printing.[25] The doped thin films prepared by these techniques are often subject to phase separation, that is, aggregation of the dopants within the thin films. The aggregation of phosphorescent iridium complexes doped in conjugated-polymer thin films has been observed by optical and atomic force microscopies[23,24,26] and can be expected to reduce the emission efficiency of the dopants through concentration quenching.[9] To counteract this phenomenon, solution processible electrophosphorescent iridium complexes have been prepared by attaching solubilizing alkyl chains[24,27] or by incorporation into dendrons.[28,29] Other solution processible conjugated electrophosphorescent iridium complexes have been reported.[30,31] We have recently reported green- and red-emitting solution processible electrophosphorescent polymers in which the iridium complex is conjugatively linked to a polyfluorene host and have shown that devices made using the covalently linked polymer outperform those made with a blend of the corresponding iridium complex in a polyfluorene host.[32] Yang and Cao have described an efficient variant using an alternating fluorene−carbazole copolymer host,[33] and Ma and colleagues have prepared a long wavelength emitting electrophosphorescent polymer by complexing a bipyridyl fluorene copolymer with rhenium.[34]

An alternative strategy for preventing phase separation is to employ a nonconjugated covalent linkage between the phosphorescent dopant and the polymer host. Copolymeric polystyrene hosts with tunable charge transporting side chains can be prepared by copolymerization with various vinyl monomers. Post polymerization modification with platinum complexes produced efficient white electrophosphorescence;[35] inclusion of an iridium complex tethered to a vinyl monomer afforded green emissive materials.[36] If the polymer host is itself conjugated, the emissive complex can be nonconjugatively linked by a tether. Examples included tethered ruthenium,[37] europium,[38] and iridium[39,40] complexes with impressive device efficiencies.

The promising results described above with covalently linked electrophosphorescent complexes in polymer hosts raises the question of the importance of spatial confinement, phase separation, relative content of the phosphorescent guest, and aggregation phenomena in designing efficient next generation materials for solid-state electroluminescence. In this paper, we describe a systematic study of the dependence of device efficiency on tether length in solution processible conjugated host fluorene copolymers carrying a pendant [Ir(btp)$_2$(acac)] fragment (Figure 1). The efficient syntheses of fluorene monomers with spacerless or octamethylene-tethered iridium complexes attached at the 9-position are described. Chain extension of these monomers by a Suzuki polycondensation with a fluorene macromonomer afforded the required materials for study. A comparison of the photo- and electroluminescence efficiencies demonstrates the advantages of controlling the triplet energy back transfer in these materials through the inclusion of

(10) Kraft, A.; Grimsdale, A. C.; Holmes, A. B. *Angew. Chem., Int. Ed.* **1998**, *37*, 402−428.
(11) Kido, J.; Nagai, K.; Ohashi, Y. *Chem. Lett.* **1990**, 657−660.
(12) Baldo, M. A.; O'Brien, D. F.; You, Y.; Shoustikov, A.; Sibley, S.; Thompson, M. E.; Forrest, S. R. *Nature* **1998**, *395*, 151−154.
(13) Kwong, R. C.; Sibley, S.; Dubovoy, T.; Baldo, M.; Forrest, S. R.; Thompson, M. E. *Chem. Mater.* **1999**, *11*, 3709−3713.
(14) Holder, E.; Langeveld, B. M. W.; Schubert, U. S. *Adv. Mater.* **2005**, *17*, 1109−1121.
(15) Adachi, C.; Baldo, M. A.; Thompson, M. E.; Forrest, S. R. *J. Appl. Phys.* **2001**, *90*, 5048−5051.
(16) Cleave, V.; Yahioglu, G.; Le Barny, P.; Hwang, D.-H.; Holmes, A. B.; Friend, R. H.; Tessler, N. *Adv. Mater.* **2001**, *13*, 44−47.
(17) Lane, P. A.; Palilis, L. C.; O'Brien, D. F.; Giebeler, C.; Cadby, A. J.; Lidzey, D. G.; Campbell, A. J.; Blau, W.; Bradley, D. D. C. *Phys. Rev. B* **2001**, *63*, 235206.
(18) Moliton, A.; Hiorns, R. C. *Polym. Int.* **2004**, *53*, 1397−1412.
(19) Van Dijken, A.; Bastiaansen, J. J. A. M.; Kiggen, N. M. M.; Langeveld, B. M. W.; Rothe, C.; Monkman, A.; Bach, I.; Stossel, P.; Brunner, K. *J. Am. Chem. Soc.* **2004**, *126*, 7718−7727.
(20) Chan, K. L.; Watkins, S. E.; Mak, C. S. K.; McKiernan, M. J.; Towns, C. R.; Pascu, S. I.; Holmes, A. B. *Chem. Commun.* **2005**, 5766−5768.
(21) Köhler, A.; Beljonne, D. *Adv. Funct. Mater.* **2004**, 14, 11−18.
(22) Hertel, D.; Setayesh, S.; Nothofer, H.-G.; Scherf, U.; Müllen, K.; Bässler, H. *Adv. Mater.* **2001**, *13*, 65−70.
(23) Chen, F.-C.; He, G.; Yang, Y. *Appl. Phys. Lett.* **2003**, *82*, 1006−1008.
(24) Chen, F.-C.; Chang, S.-C.; He, G.; Pyo, S.; Yang, Y.; Kurotaki, M.; Kido, J. *J. Polym. Sci., Part B: Polym. Phys.* **2003**, *41*, 2681−2690.
(25) Friend, R. H.; et al. *Nature* **1999**, *397*, 121−128.
(26) Noh, Y.-Y.; Lee, C.-L.; Kim, J.-J.; Yase, K. *J. Chem. Phys.* **2003**, *118*, 2853−2864.
(27) Zhu, W.; Liu, C.; Su, L.; Yang, W.; Yuan, M.; Cao, Y. *J. Mater. Chem.* **2003**, *13*, 50−55.
(28) Lo, S.-C.; Namdas, E. B.; Burn, P. L.; Samuel, I. D. W. *Macromolecules* **2003**, *36*, 9721−9730.
(29) Anthopoulos, T. D.; Markham, J. P. J.; Namdas, E. B.; Lawrence, J. R.; Samuel, I. D. W.; Lo, S.-C.; Burn, P. L. *Org. Electron.* **2003**, *4*, 71−76.
(30) Ostrowski, J. C.; Robinson, M. R.; Heeger, A. J.; Bazan, G. C. *Chem. Commun.* **2002**, 784−785.
(31) Gong, X.; Ostrowski, J. C.; Moses, D.; Bazan, G. C.; Heeger, A. J. *J. Polym. Sci., Part B: Polym. Phys.* **2003**, *41*, 2691−2705.
(32) Sandee, A. J.; Williams, C. K.; Evans, N. R.; Davies, J. E.; Boothby, C. E.; Köhler, A.; Friend, R. H.; Holmes, A. B. *J. Am. Chem. Soc.* **2004**, *126*, 7041−7048.
(33) Zhen, H.; Jiang, C.; Yang, W.; Jiang, J.; Huang, F.; Cao, Y. *Chem.—Eur. J.* **2005**, *11*, 5007−5016.
(34) Zhang, M.; et al. *J. Phys. Chem. B* **2004**, *108*, 13185−13190.
(35) Furuta, P. T.; Deng, L.; Garon, S.; Thompson, M. E.; Fréchet, J. M. J *J. Am. Chem. Soc.* **2004**, *126*, 15388−15389.
(36) Suzuki, M.; Tokito, S.; Sato, F.; Igarashi, T.; Kondo, K.; Koyama, T.; Yamaguchi, T. *Appl. Phys. Lett.* **2005**, *86*, 103507.
(37) Wong, C. T.; Chan, W. K. *Adv. Mater.* **1999**, *11*, 455−459.
(38) Pei, J.; Liu, X.-L.; Yu, W.-L.; Lai, Y.-H.; Niu, Y.-H.; Cao, Y. *Macromolecules* **2002**, *35*, 7274−7280.
(39) Chen, X.; Liao, J.-L.; Liang, Y.; Ahmed, M. O.; Tseng, H.-E.; Chen, S.-A. *J. Am. Chem. Soc.* **2003**, *125*, 636−637.
(40) Jiang, J.; Jiang, C.; Yang, W.; Zhen, H.; Huang, F.; Cao, Y. *Macromolecules* **2005**, *38*, 4072−4080.

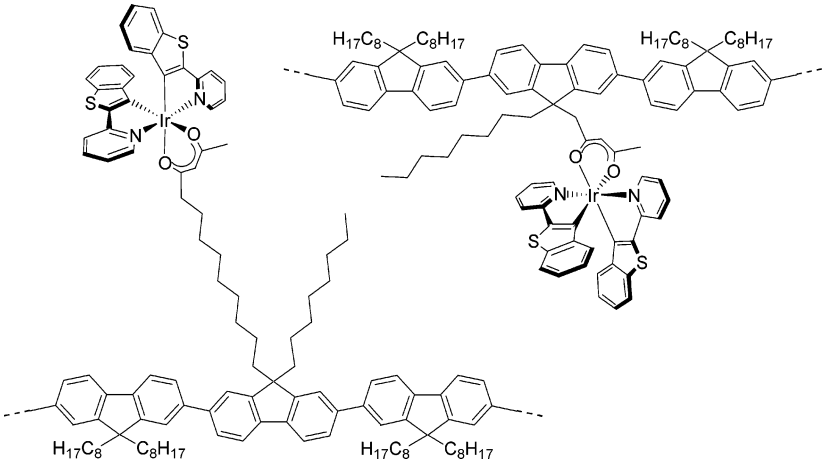

Figure 1. The key structural motifs of the copolymers with and without alkyl spacers (tethers) between the polyfluorene chains and pendant red phosphorescent iridium complexes.

Scheme 1. Synthetic Route to the Octamethylene-Tethered Ligand **6**[a]

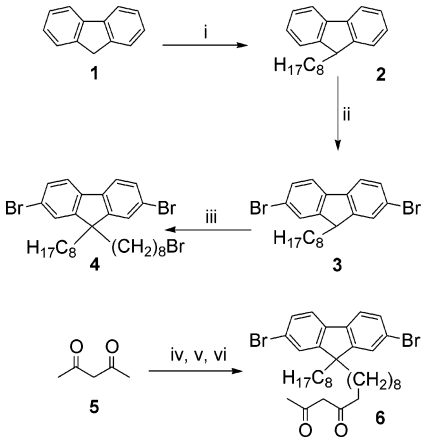

[a] Reagents and conditions: (i) octan-1-ol, KOH, air, 190 °C, 96%; (ii) Br_2, I_2, DCM, dark, 0 °C → room temperature, 90%; (iii) $Br(CH_2)_8Br$, aq. NaOH, Aliquat 336, 80 °C, 71%; (iv) NaH, THF, 0 °C; (v) BuLi, 0 °C; (vi) **4**, 0 °C → room temperature, 58%.

an octamethylene linking group. Together with recent studies of the relative efficiencies of blends and the above-mentioned copolymer systems, this work provides further insight into the design criteria for materials in electrophosphorescent conjugated-polymer OLEDs.

Results and Discussion

Synthesis and Characterization. Syntheses of the octamethylene-tethered monomer **8**, the spacerless monomer **12**, and the corresponding phosphorescent copolymers **17** and **18** are reported. X-ray crystal structures of the iridium complexes **12** and **13** provide useful information about spatial arrangements in the crystals.

The Octamethylene-Tethered Monomer 8. The synthesis of the functionalized fluorene **6** carrying the octamethylene-tethered pentanedione unit is shown in Scheme 1. 9-Octylfluorene **2** was prepared in 96% yield by the base-mediated alkylation[41,42] of 9*H*-fluorene with octanol. Bromination of 9-octyl-9*H*-fluorene **2** gave 2,7-dibromo-9-octyl-9*H*-fluorene **3**[43] in 90% yield. Alkylation of the dibromide **3** with 10 equiv of 1,8-dibromooctane under alkaline phase-transfer conditions afforded the 8′-bromooctyl derivative **4** in 71% yield. Treatment of the bisenolate of pentane-2,4-dione **5**[44] with **4** provided the octamethylene-tethered ligand **6** in 58% yield.

Formation of the iridium complex **8** by reaction of the diketone **6** with the crude chloro-bridged iridium dimer **7**[45] and sodium carbonate in 2-ethoxyethanol under reflux overnight[39] or at a lower temperature of 80 °C was accompanied by hydrodebrominated derivatives, as evidenced by a signal at δ 7.30−7.35 in the ^{1}H NMR spectrum of the product in *d*-chloroform and a discordant elemental analysis (see Figure S1 and the Supporting Information). These could be formed by a radical-chain, electron-transfer mechanism that accounts for alkoxide-mediated hydrodebromination.[46,47] A possible source of radical initiation under these conditions is unclear, although cyclometalated iridium complexes are known to be powerful single-electron donors.[48] This side reaction was overcome by carrying out the complexation reaction in a nonalcoholic solvent. Reaction of the octamethylene-tethered ligand **6** with the crude dimer **7** and sodium carbonate in acetonitrile at 80 °C provided the octamethylene-tethered monomer **8** in ca. 74% yield after purification by chromatography, as shown in Scheme 2. The ^{1}H NMR spectrum of the octamethylene-tethered monomer **8** prepared under these conditions exhibits only a trace of hydrodebrominated impurities, and the elemental analysis of the product is consistent with that expected for the octamethylene-tethered monomer **8** (see Figure S2 and the Supporting Information). We have found that acetonitrile as the reaction solvent also affords a cleaner complexation of the chloro-bridged iridium dimer **7** with sodium carbonate and other β-diketones in general, greatly simplifying isolation of the desired phosphorescent complexes.

The Spacerless Monomer 12. The synthesis of the spacerless monomer **12** using 6-bromomethyl-4-methoxy-2*H*-pyran-2-one **9**[49] as a latent 1-bromopentane-2,4-dione electrophile is il-

(41) Schoen, K. L.; Becker, E. I. *J. Am. Chem. Soc.* **1955**, *77*, 6030−6031.
(42) Fritz, H. E.; Peck, D. W.; Eccles, M. A.; Atkins, K. E. *J. Org. Chem.* **1965**, *30*, 2540−2542.
(43) Ego, C.; Marsitzky, D.; Becker, S.; Zhang, J.; Grimsdale, A. C.; Müllen, K.; MacKenzie, J. D.; Silva, C.; Friend, R. H. *J. Am. Chem. Soc.* **2003**, *125*, 437−443.
(44) Hauser, C. R.; Harris, T. M. *J. Am. Chem. Soc.* **1958**, *80*, 6360−6363.
(45) Lamansky, S.; Djurovich, P.; Murphy, D.; Abdel-Razzaq, F.; Lee, H.-E.; Adachi, C.; Burrows, P. E.; Forrest, S. R.; Thompson, M. E. *J. Am. Chem. Soc.* **2001**, *123*, 4304−4312.
(46) Bunnett, J. F.; Wamser, C. C. *J. Am. Chem. Soc.* **1967**, *89*, 6712−6718.
(47) Bunnett, J. F. *Acc. Chem. Res.* **1992**, *25*, 2−9.
(48) Yuasa, J.; Suenobu, T.; Fukuzumi, S. *J. Am. Chem. Soc.* **2003**, *125*, 12090−12091.

Scheme 2. Synthesis of the Octamethylene-Tethered Monomer **8**[a]

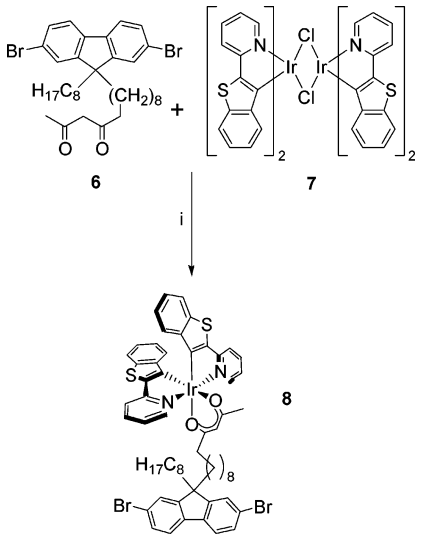

[a] Reagents and conditions: (i) Na_2CO_3, acetonitrile, 80 °C, 48 h, ca. 74%.

lustrated in Scheme 3. 2,7-Dibromo-9-octyl-9*H*-fluorene **3** was deprotonated with LDA and treated with the crude bromopyrone **9** to provide the pyrone **10** in ca. 87% yield. Hydrolysis and decarboxylation of the pyrone **10** afforded the dione **11**. Unfortunately, the dione **11** could not be separated from an unidentified byproduct by chromatography or distillation. The conversion of the pyrone **10** into the dione **11** was estimated to be ca. 69% from ^{1}H NMR data. Fortunately, the byproduct was itself not a dione and thus did not interfere in the subsequent complexation of the dione **11** with the crude chloro-bridged iridium dimer **7** and sodium carbonate in acetonitrile at 80 °C to yield the spacerless monomer **12** in ca. 81% yield after chromatographic purification.

Van Dijken et al. have shown that phosphorescent iridium complexes with dionate ligands decompose upon contact with poly(3,4-ethylenedioxythiophene):poly(styrenesulfonate) (PEDOT:PSS), in both solid and solution.[50] Treatment of a solution of the spacerless monomer **12** in dichloromethane−acetonitrile in the presence of *p*-toluenesulfonic acid monohydrate, chosen to mimic the acidic action of PEDOT:PSS, regenerated the dione **11** in quantitative yield. This decomposition gave pure **11** which enabled its full characterization (see the Supporting Information). This transformation supports the notion that a PEDOT:PSS layer could be detrimental in devices of phosphorescent iridium complexes with diketonate ligands.[50] An improvement in the efficiency of red phosphorescent polyfluorene OLEDs has been demonstrated recently with the use of an alternative hole-injection layer to that of PEDOT:PSS, and an additional hole-blocking layer.[51]

The X-ray crystal structure of the spacerless monomer **12** is represented in Figure 2. The C−Ir−N bite angles are 80.74(16) and 79.99(17)° for the cyclometalating ligands closest and furthest from the fluorenyl group, respectively, and 89.79(12)° for the dionate ligand, with a 178.81(9)° bond angle between the coordinating nitrogen atoms, N(1)−Ir(1)−N(2). These angles, and the corresponding coordination bond lengths, are within the same range as those found in the original[45] red phosphorescent iridium complex **13** (see Chart 1), as well as other related iridium complexes[52] (see the Supporting Information). The spacerless monomer **12** adopts a face-to-face conformation of the iridium complex and fluorenyl group in the crystalline state. This conformation, with a separation of only 3.6 Å between cyclometalating ligand and fluorenyl group at the closest point, is expected to facilitate $\pi-\pi$ interactions between these parts of the spacerless monomer **12**.[53] Such orbital interactions are known to be the key requirement for Dexter triplet energy transfer.[54]

A ^{1}H−^{1}H COSY NMR spectrum enables the near-complete assignment of all the aromatic protons for the spacerless monomer **12** in *d*-chloroform (with only the sense of the benzo[*b*]thienyl protons and the pairings of pyridyl and benzo[*b*]thienyl ring systems undetermined with this technique; see Figure S3). The pyridyl α-protons of the spacerless monomer **12** are observed as doublets at δ 7.20 (J = 5.4 Hz) and δ 8.13 (J = 5.6 Hz), which are consistent with the spacerless monomer **12** also adopting a face-to-face conformation of the iridium complex and fluorenyl group (for at least part of the time) in solution. The pyridyl α-proton directed toward the face of the fluorenyl group (δ 7.20) is shielded by the ring-current effect of the fluorenyl group. Thus, our design for the spacerless monomer **12** is expected to facilitate Dexter triplet energy transfer between the polyfluorene chain and the adjoining red phosphorescent iridium complex in our spacerless conjugated copolymer systems.

Phosphorescent Copolymers. The aim of attaching a phosphorescent dopant to a host polymer is to inhibit phase separation within the system because aggregation of the dopant is expected to reduce the phosphorescence efficiency through concentration quenching. Covalent attachment also provides solution processible polymeric iridium complexes and spatial control of the orientation of the metal complex with respect to the host polymer. Although a chance (or otherwise) meeting between dopants attached to separate copolymer chains cannot be avoided in a solid thin film, contact between dopants attached to the same copolymer chain can at least be minimized. The distribution of the phosphorescent monomer within the copolymer chain is determined in part by the relative incorporation rates of the phosphorescent and conventional monomers, giving rise to composition drift.[55] If the incorporation rate is faster for the phosphorescent monomer than for the conventional monomers, then a higher frequency of dopants can be expected in those chains generated earlier in the copolymerization, providing undesirably close contact between some dopants. Alternatively, if the reactivity of the phosphorescent monomers is lower than that of the conventional monomers, then incorporation of the dopants may be incomplete, as the concentration of reactive end groups decreases toward the termination of the copolymerization. To achieve an even distribution of phosphorescent monomers within a copolymer, the approach was to conduct a

(49) Bloomer, J. L.; Zaidi, S. M. H.; Strupczewski, J. T.; Brosz, C. S.; Gudzyk, L. A. *J. Org. Chem.* **1974**, *39*, 3615−3616.
(50) Van Dijken, A.; Perro, A.; Meulenkamp, E. A.; Brunner, K. *Org. Electron.* **2003**, *4*, 131−141.
(51) Niu, Y.-H.; et al. *Appl. Phys. Lett.* **2004**, *85*, 1619−1621.
(52) Lamansky, S.; Djurovich, P.; Murphy, D.; Abdel-Razzaq, F.; Kwong, R.; Tsyba, I.; Bortz, M.; Mui, B.; Bau, R.; Thompson, M. E. *Inorg. Chem.* **2001**, *40*, 1704−1711.
(53) Hunter, C. A.; Sanders, J. K. M. *J. Am. Chem. Soc.* **1990**, *112*, 5525−5534.
(54) Klessinger, M.; Michl, J. *Excited States and Photochemistry of Organic Molecules*; VCH Publishers: New York, 1995.
(55) Cowie, J. M. G. *Polymers: Chemistry and Physics of Modern Materials*, 2nd ed.; Stanley Thornes: Cheltenham, UK, 1998.

Scheme 3. Synthesis of the Spacerless Monomer **12**[a]

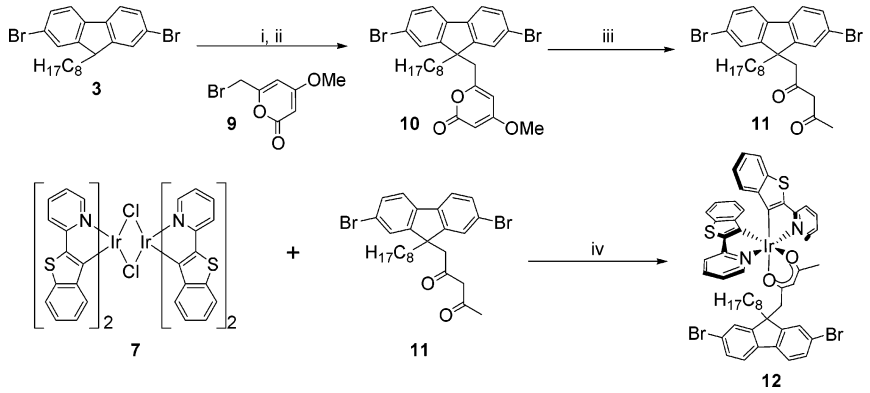

[a] Reagents and conditions: (i) LDA, THF, −78 °C; (ii) crude **9**, −78 °C → room temperature, ca. 87%; (iii) aq. HCl, acetic acid, 100 °C, ca. 69% crude; (iv) Na_2CO_3, acetonitrile, 80 °C, 48 h, ca. 81%.

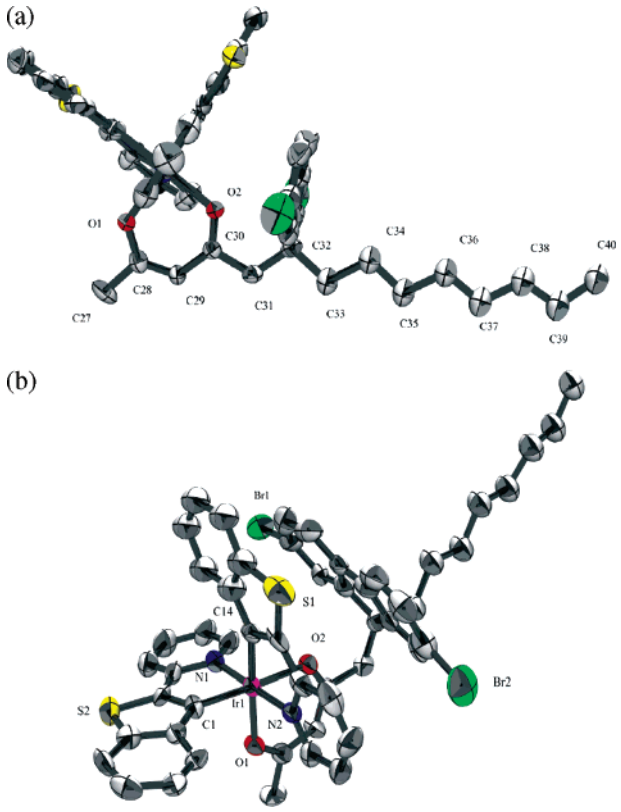

Figure 2. (a) X-ray crystal structure of the spacerless monomer **12**, showing the pertinent atom labels. (b) Alternative view showing the octahedral coordination environment at the metal center. Displacement ellipsoids are drawn at the 40% probability level. Hydrogen atoms and solvent have been omitted for clarity.

Chart 1. The Red Phosphorescent Iridium Complex **13**

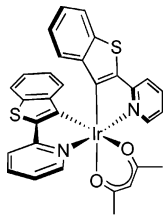

13

step-growth copolymerization in stages. Here, in the first stage, the conventional fluorene monomers **14** and **15** were combined in a ratio so as to generate a macromonomer **16** that retains an excess of reactive boronic ester end groups (Scheme 4). In the second stage, the spacerless monomer **12** or the octamethylene-tethered monomer **8** was chain extended by copolymerization with the macromonomer **16** and end-capped by the solvent, chlorobenzene, to give the phosphorescent copolymers **17** and **18**, respectively (Scheme 5).

Scheme 4. Synthesis of the Macromonomers **16a** and **16b**[a]

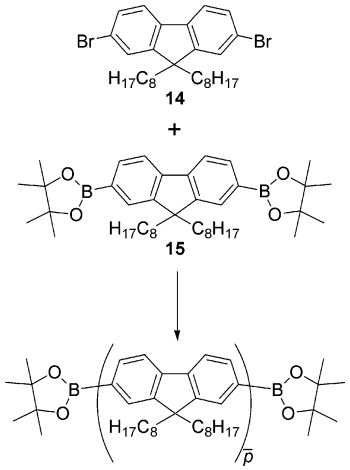

16a (**14**:**15** = 1.11:1.00, $\bar{p}$ = 16)
16b (**14**:**15** = 1.14:1.00, $\bar{p}$ = 15)

[a] Reagents and conditions: (i) $Pd(OAc)_2$, PCy_3, toluene, aq. Et_4NOH, 90 °C, 2 h, **16a** ca. 98%, **16b** ca. 95%. Values for the structural variable *p* are estimates from ^1H NMR data (see Table 1 and the Supporting Information).

The iridium complex loadings and molecular weights of the phosphorescent copolymers **17** and **18** were controlled through the average chain length of the macromonomer **16**. The macromonomers **16a** and **16b** were prepared by the Suzuki polycondensation[56] of the bis(boronic ester) **14** and the dibromide **15**, as shown in Scheme 4. The bis(boronic ester) **14** and the dibromide **15** were combined in a molar ratio of 1.11:1.00 (for an expected average degree of polymerization, $\bar{x}_n$, of 19; see the Supporting Information) to give the longer macromonomer **16a**, and 1.14:1.00 (expected $\bar{x}_n$ of 15) to give the shorter macromonomer **16b**. The proportion of catalyst, palladium(II) acetate, and tricyclohexylphosphine (1:5 molar ratio) was 1 mol

(56) Schlüter, A. D. *J. Polym. Sci., Part A: Polym. Chem.* **2001**, *39*, 1533−1556.

Scheme 5. Synthesis of the Spacerless Copolymers, **17a** and **17b**, and the Octamethylene-Tethered Copolymers, **18a** and **18b**, by Chain Extension of the Monomers **12** and **8**, Respectively, with the Macromonomer **16**[a]

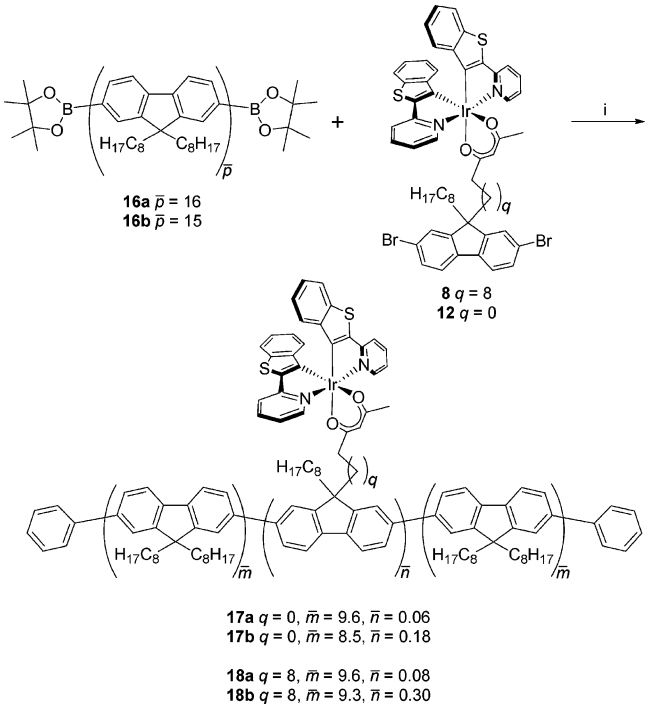

[a] Reagents and conditions: (i) $Pd(OAc)_2$, PCy_3, chlorobenzene, aq. Et_4NOH, 90 °C, 2 h, **17a** ca. 77%, **17b** ca. 86%, **18a** ca. 76%, **18b** ca. 78%. Values for the structural variables $\bar{m}$, $\bar{n}$, and $\bar{p}$ are estimates from ^1H NMR data (see Table 1 and the Supporting Information).

% with respect to the bis(boronic ester) **14**.[57] This polycondensation stage was conducted in a biphasic mixture of toluene and aqueous tetraethylammonium hydroxide at 90 °C with vigorous stirring for 2 h,[58] before the crude macromonomer **16** was isolated in high yield as green fibers by precipitation from methanol. The values for $\bar{x}_n$ that have been estimated from ^1H NMR data, ca. 16 and 15 for the macromonomers **16a** and **16b**, respectively, are similar to the expected values (see the Supporting Information).

Unfortunately, toluene is a poor solvent for the second stage of the Suzuki polycondensation reaction; the solubility of the spacerless monomer **12** is only 0.6 mg cm^{-3} in toluene at room temperature. A more useful solvent for the spacerless monomer **12** is chlorobenzene (the solubility of **12** is 2 mg cm^{-3} at room temperature). The second stage of synthesizing the spacerless copolymers **17a** and **17b** is illustrated in Scheme 5. The spacerless monomer **12** was chain extended by copolymerization with 10 molar equiv of the macromonomer **16a**, or 3.9 molar equiv of the macromonomer **16b**, under conditions identical to those of the first stage, except the reaction solvent was chlorobenzene rather than toluene. Chlorobenzene is both solvent and end-capping reagent. The spacerless copolymers **17a** and **17b** were isolated by precipitation from methanol and purified by filtration through silica followed by precipitation from methanol to afford good yields of the copolymers as yellow and orange fibers, respectively. The octamethylene-tethered copolymers **18a** and **18b** were obtained as yellow and orange fibers, respectively, in good yields. (The octamethylene-tethered monomer **8** dissolves readily in toluene—solubility greater than 100 mg cm^{-3} at room temperature. A toluene solution of the octamethylene-tethered monomer **8** can be added directly to the polycondensation reaction, without isolation of the macromonomer **16**, as the second stage in an alternative, one-pot copolymerization. The iridium complex loadings of the octamethylene-tethered copolymers **18a** and **18b** synthesized in chlorobenzene are comparable to those of the analogous copolymers synthesized in toluene.)

Characterization of the Iridium-Tethered Copolymers. The loadings of iridium complex in the phosphorescent copolymers **17** and **18** were investigated through elemental and ^1H NMR analyses, and the results are summarized in Table 1. Carbon, hydrogen, and nitrogen elemental analyses of the products are consistent with those expected for the copolymers, given the accustomed margin of accuracy (±0.3% points). The idealized representations of the copolymers in Scheme 5 are characterized by the structural variables $\bar{m}$ and $\bar{n}$, and values for these variables have been estimated from ^1H NMR data (see the Supporting Information). The iridium complex loading of each copolymer can be more conveniently expressed as the weight-percentage of the red phosphorescent iridium complex **13** calculated from the mole fraction of the attached iridium complex of the copolymer. The iridium complex loadings estimated for the spacerless copolymers **17a** and **17b** are noticeably less than those estimated for the corresponding octamethylene-tethered copolymers **18a** and **18b** (see Table 1). This may only be a result of inaccuracies in the integration processes (a broadening of the iridium complex dionate methine signal into the spectral noise almost certainly contributes to an underestimation of the iridium complex loadings in the spacerless copolymers **17a** and **17b** by this method; cf. Figures S4 and S5), but it may also reflect a true difference in the iridium complex loadings of the copolymers. This could result from a slower reactivity of the spacerless monomer **12** in the Suzuki polycondensation reaction compared with the octamethylene-tethered monomer **8**.

The molecular weights of the phosphorescent copolymers **17** and **18** were investigated through ^1H NMR and gel-permeation chromatography (GPC), and the results are summarized in Table 1. Values for $\bar{x}_n$ of 17−19 were estimated from ^1H NMR data (see the Supporting Information), which are lower than the value of 21 intended for these copolymers. GPC analyses were performed in THF at 30 °C against a calibration with polystyrene standards. The observed values for $\bar{M}_n$ are about twice those expected, which is consistent with previous reports of a polystyrene calibration providing an overestimate of the molecular weight for poly(9,9-dioctyl-9*H*-fluorene-2,7-diyl) (PFO).[59]

Thermal analysis of the phosphorescent copolymers **17** and **18** was performed with differential scanning calorimetry (DSC) and thermogravimetric analysis (TGA), and the results are summarized in Table 1. Glass, melting, and crystallization transitions have been observed at comparable temperatures in PFO.[60] IR and ^{13}C NMR spectra and MALDI mass spectrometry data were measured. The MALDI analyses revealed that the

(57) Holmes, A. B.; Martin, R. E.; Ma, Y.; Rees, I. D.; Cacialli, F.; Fischmeister, C. WO 26 856/2002 (*Chem. Abstr.* **2002**, *136*, 295241).
(58) Towns, C. R.; O'Dell, R. WO 53 656/2000 (*Chem. Abstr.* **2000**, *133*, 238529).
(59) Grell, M.; Bradley, D. D. C.; Long, X.; Chamberlain, T.; Inbasekaran, M.; Woo, E. P.; Soliman, M. *Acta Polym.* **1998**, *49*, 439−444.
(60) Grell, M.; Bradley, D. D. C.; Inbasekaran, M.; Woo, E. P. *Adv. Mater.* **1997**, *9*, 798−802.

Table 1. Characterization of the Spacerless Copolymers **17a** and **17b** and the Octamethylene-Tethered Copolymers **18a** and **18b**

copolymer		17a	17b	18a	18b
approximate yield (%)		77	86	76	78
elemental analysis (%)[a]	C	89.3 (89.3)	88.6 (88.6)	89.4 (89.3)	88.8 (88.6)
	H	10.2 (10.2)	10.2 (10.1)	10.2 (10.2)	10.2 (10.1)
	N	0.09 (0.04)	0.26 (0.12)	0.11 (0.04)	0.25 (0.12)
expected from stoichiometry[b]	$\bar{x}_n$	21	21	21	21
	$\bar{m}$	10	10	10	10
	$\bar{n}$	0.12	0.36	0.12	0.36
	wt % **13**	1.0	3.0	1.0	3.0
calcd from ^{1}H NMR integrals[b]	$\bar{x}_n$	19	17	19	19
	$\bar{m}$	9.6	8.5	9.6	9.3
	$\bar{n}$	0.06	0.18	0.08	0.30
	wt % **13**	0.6	1.8	0.7	2.8
GPC[c]	$\bar{M}_n$	17000	20000	16000	18000
	M_p	46000	48000	38000	48000
	$\bar{M}_w$	43000	50000	42000	48000
	PDI	2.6	2.6	2.6	2.6
DSC (°C)[d]	T_g	60−68	65−74	64−73	65−74
	T_c	106	115	104	109
	T_m	129, 145	136	128, 145	131, 142
TGA (°C)[e]	T_d	309	349	335	325

[a] Values calculated for the copolymer structures expected from the reaction stoichiometries are given in parentheses. [b] The variables $\bar{m}$ and $\bar{n}$ are the structural variables in Scheme 5; $\bar{x}_n$ is the number-average degree of polymerization. The iridium complex loading is expressed as the weight-percentage of the equivalent red phosphorescent complex **13** calculated from the mole fraction of the iridium complex attached to the copolymer. [c] Gel-permeation chromatography. $\bar{M}_n$, M_p, and $\bar{M}_w$ are the number-average, peak and weight-average molecular weights, respectively, referenced against a calibration with polystyrene standards. PDI is the polydispersity index. [d] Differential scanning calorimetry. T_g is the glass transition temperature range. T_c and T_m are the peak maximum crystallization and melting temperatures, respectively. [e] Thermogravimetric analysis. T_d is the trigger-point decomposition temperature for 0.5% mass loss.

copolymers consisted predominantly of chains with odd numbers of fluorenyl units (because an excess of the monomer **14** over the monomer **15** was used in preparing the macromonomers **16)**, and a fraction (typically 7−16% for the odd-numbered series) of hydrogen, rather than phenyl, end groups.[61] Ions consistent with chains bonded with iridium complexes were observed for the copolymers with higher iridium complex loadings (**17b** and **18b**). The MALDI analyses provide underestimates for the molecular weight distributions of the copolymers ($\bar{M}_n$ 2800−3200, $\bar{M}_w$ 3400−4100, PDI 1.2−1.3; see the Supporting Information) because of a bias toward lower molecular weight fractions in polydisperse samples.[62]

Optical Spectroscopy. Absorption Spectra. The normalized absorption spectra of thin films of the phosphorescent copolymers **17** and **18** are presented in Figure 3. The spectra are very similar to the absorption spectrum of PFO,[63] with maxima centered at 3.17 eV (391 nm) for the octamethylene-tethered copolymer **18b** and 3.23 eV (384 nm) for the other polymers. The small shoulder at 2.85 eV (435 nm) in the spectra of **18b** and PFO indicates the presence of a small fraction of planarized chain conformations in these films.[63,64] This feature is much weaker in the spectra of the spacerless copolymers **17**, indicating that a direct connection of the iridium complex to the polyfluorene backbone inhibits planarization in these films. The slightly lower energy of the absorption maximum in the octamethylene-tethered copolymer **18b** is attributed to the effect of this planarization. Our observation that the absorption maxima of the copolymers **17** and **18** essentially coincide with that of PFO is consistent with an estimate of the effective conjugation length in polyfluorenes being only 12 bonded fluorene units[65] and justifies the study of the relatively low-molecular-weight copolymers **17** and **18** as models for PFO. We also note that the contribution of the bonded iridium complexes to the absorption spectra of the copolymers **17** and **18** is too weak to be distinguished from the scattering in the baseline; it is therefore not possible to derive information on the iridium complex loadings in the copolymers **17** and **18** from their absorption spectra.

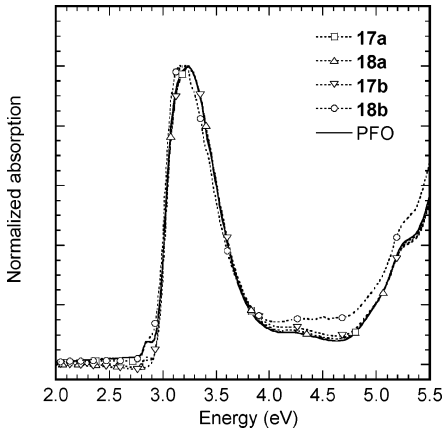

Figure 3. The thin film absorption spectra of the spacerless copolymers **17a** and **17b** and the octamethylene-tethered copolymers **18a** and **18b** and poly(9,9-dioctyl-9*H*-fluorene-2,7-diyl) (PFO) at room temperature.

Photoluminescence and Electroluminescence Properties. The room-temperature photoluminescence (PL) spectra for the

(61) Chen, H.; He, M.; Pei, J.; Liu, B. *Anal. Chem.* **2002**, *74*, 6252−6258.
(62) Martin, K.; Spickermann, J.; Räder, H. J.; Müllen, K. *Rapid Commun. Mass Spectrom.* **1996**, *10*, 1471−1474.
(63) Khan, A. L. T.; Sreearunothai, P.; Herz, L. M.; Banach, M. J.; Köhler, A. *Phys. Rev. B: Condens. Matter* **2004**, *69*, 085201.
(64) Grell, M.; Bradley, D. D. C.; Ungar, G.; Hill, J.; Whitehead, K. S. *Macromolecules* **1999**, *32*, 5810−5817.
(65) Klaerner, G.; Miller, R. D. *Macromolecules* **1998**, *31*, 2007−2009.

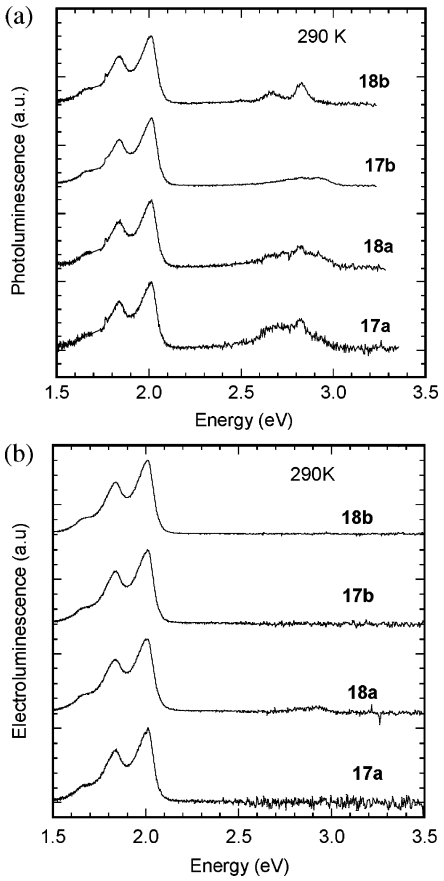

Figure 4. The thin film (a) photoluminescence (PL) and (b) electroluminescence (EL) spectra of the spacerless copolymers **17a** and **17b** and octamethylene-tethered copolymers **18a** and **18b** at room temperature. The spectra are normalized and offset along the vertical axis. Optical excitation for the PL spectra was provided by the 355 and 364 nm lines of an Ar^+ laser.

phosphorescent copolymers **17** and **18** are presented in Figure 4a. The room-temperature PL is characterized by both fluorescence from the polyfluorene backbone [with a peak around 2.8 eV (443 nm)] and phosphorescence from the bonded iridium complex [with a peak around 2.0 eV (620 nm)].[32] OLEDs with simple device structures of glass/ITO/PEDOT:PSS/copolymer/Ca/Al were fabricated for the copolymers **17** and **18** (see the Supporting Information), and the electroluminescence (EL) spectra are presented in Figure 4b. The EL spectra are almost identical for all four copolymers because the emission from the triplet state of the iridium complex is observed with little or no singlet emission from the polyfluorene chains.[32] This indicates that charge trapping rather than energy transfer is the predominant mechanism of EL in these devices.[66,67] Under electrical excitation, the holes and electrons are expected to be trapped by the iridium complexes in the copolymers **17** and **18** because both the HOMO (−5.1 eV) and LUMO (−2.4 eV) energy levels reported for the model red phosphorescent iridium complex **13** lie inside those of PFO (HOMO −5.6 eV and LUMO −2.2 eV).[39]

The phosphorescence quantum efficiencies for thin films of the phosphorescent copolymers **17** and **18** are listed in Table 2. The efficiency increases with the iridium complex loading in both the copolymers **17** and **18**. More importantly, we find that the phosphorescence efficiencies of the octamethylene-tethered copolymers **18a** and **18b** are approximately double those of the corresponding spacerless copolymers **17a** and **17b**. The greater efficiencies of the octamethylene-tethered copolymers **18** cannot be attributed entirely to the somewhat higher iridium complex loadings estimated for **18** from ^{1}H NMR data: the phosphorescence efficiency ([22 ± 4]%) of the octamethylene-tethered copolymer **18a** (iridium complex loading of 0.7 wt %) is similar to that ([19 ± 4]%) of the spacerless copolymer **17b** even though **17b** has a higher iridium complex loading (1.8 wt %). The external EL quantum efficiencies at 100 cd m^{-2} for OLEDs of the phosphorescent copolymers **17** and **18** are also listed in Table 2 and for the most part follow a similar pattern: the EL efficiency of the octamethylene-tethered copolymer **18a** is about twice that of the corresponding spacerless copolymer **17a** and still greater than that of the spacerless copolymer **17b** with a higher iridium complex loading. However, in contrast to the PL efficiency data, the EL efficiency of the octamethylene-tethered copolymer **18b** is the same (within experimental error) as those of the spacerless copolymer **17b** and the other octamethylene-tethered copolymer **18a**. Further details about the PL and EL efficiency are given in the Supporting Information.

We consider this unexpected low EL efficiency of **18b** may be a consequence of triplet−triplet annihilation. Measurements by Gong and co-workers on polyfluorene doped with iridium complexes have shown that triplet−triplet annihilation begins to occur for doping concentrations above 1−2 wt %.[66] The content of iridium complex in **18b** is about 3 wt %, so the EL QY is therefore likely to be affected by triplet−triplet annihilation in contrast to the other copolymers **17a**, **17b,** and **18a** that have lower iridium complex loadings of 0.6−1.8 wt %. This is different from the measurements of PL QY, where excitation densities are low enough to prevent triplet−triplet annihilation.

The difference in EL efficiency between the spacerless copolymer **17a** and the octamethylene-tethered copolymer **18a** is striking. Given that the mechanism for creating excitons under electrical excitation is charge trapping on the iridium complex, then the same number of excitons should be created in **17a** as in **18a**. This raises the question of why the luminescence efficiency depends on the presence or not of a spacer (tether) between the polyfluorene backbone and the bonded iridium complex.

Thompson and co-workers have shown that endothermic Dexter triplet energy transfer from phosphorescent iridium complexes to a fluorene trimer occurs very efficiently in solution. They proposed that this same process should be less efficient in a solid blend of an iridium complex and polyfluorene.[68] One of the reasons for this is the lack of molecular motion within a thin film, preventing the randomly orientated iridium complexes from adopting conformations that are more efficient for triplet energy transfer. In the phosphorescent copolymers **17** and **18**, the triplet energy levels of the bonded iridium complex and polyfluorene are similar (2.0 and 2.1 eV, respectively), and so endothermic triplet energy transfer can be expected to occur. Furthermore, crystallographic analysis of the

(66) Gong, X.; Ostrowski, J. C.; Moses, D.; Bazan, G. C.; Heeger, A. J. *Adv. Funct. Mater.* **2003**, *13*, 439−444.
(67) Gong, X.; Ostrowski, J. C.; Bazan, G. C.; Moses, D.; Heeger, A. J.; Liu, M. S.; Jen, A. K.-Y. *Adv. Mater.* **2003**, *15*, 45−49.
(68) Sudhakar, M.; Djurovich, P. I.; Hogen-Esch, T. E.; Thompson, M. E. *J. Am. Chem. Soc.* **2003**, *125*, 7796−7797.

Table 2. The Photoluminescence and Electroluminescence Quantum Yields and Photoluminescence Lifetimes along with Their Relative Contributions to Biexponential Fit for the Spacerless Copolymers **17a** and **17b** and the Octamethylene-Tethered Copolymers **18a** and **18b** in Thin Films at Room Temperature

connection	copolymer	estimated Ir complex loading (wt % **13**)[a]	phosphorescence QY (%)[b]	EL QY (%)[c]	τ_1 (μs)[d]	τ_2 (μs)[d]	I_1[d]	I_2[d]
spacerless	**17a**	0.6	12 ± 4	1.1 ± 0.1	3.8 ± 0.1	0.9 ± 0.1	0.90	0.10
tethered	**18a**	0.7	22 ± 4	2.0 ± 0.1	4.3 ± 0.1	1.5 ± 0.1	0.86	0.14
spacerless	**17b**	1.8	19 ± 4	1.7 ± 0.1	3.7 ± 0.1	0.9 ± 0.1	0.64	0.36
tethered	**18b**	2.8	40 ± 4	1.9 ± 0.1	4.0 ± 0.1	0.9 ± 0.1	0.66	0.34

[a] The iridium complex loading is expressed as the weight-percentage of equivalent red phosphorescent iridium complex **13** as calculated from the mole fraction of the attached iridium complex in the copolymer and was estimated from ^{1}H NMR data (see the Supporting Information). [b] Photoluminescence quantum yield, excitation at 355 and 364 nm. [c] Electroluminescence quantum yield at 100 cd m^{-2}. [d] Where τ and I are the photoluminescence lifetimes and relative intensity contributions, respectively, according to the biexponential decay equation: $I(t) = I_1\exp(t/\tau_1) + I_2\exp(t/\tau_2) + c$. The parameter c denotes the value of any baseline (see Figure 5 for the fits).

spacerless monomer **12** shows that a face-to-face interaction is present in the crystal with a separation of only 3.6 Å between the fluorenyl group and a cyclometalating ligand of the bonded iridium complex. Such arrangements within the spacerless copolymers **17** would encourage the wave function overlap of the frontier molecular orbitals and thus Dexter triplet energy transfer between the polyfluorene backbone and the bonded iridium complexes. As a result, triplet excitons can readily back transfer from the iridium complexes to the polyfluorene backbone in the spacerless copolymers **17** and diffuse along the polyfluorene chains to dissociation sites. In contrast, triplet excitons are confined more effectively on the iridium complex in the octamethylene-tethered copolymers **18** because the tether imposes a spatial separation between the iridium complex and polyfluorene backbone. The lower EL efficiencies of the spacerless copolymers **17** compared with those of the octamethylene-tethered copolymers **18**, in particular, for the copolymers **17a** and **18a** with lower iridium complex loadings, point to greater triplet energy back transfer from the bonded iridium complexes to their polyfluorene hosts in the spacerless copolymers **17**.

To investigate this effect further, we have measured the PL lifetime of the copolymers **17** and **18**. Figure 5 shows the decay of the PL intensity at room temperature and lines of best fit to the biexponential decay equation:

$$I(t) = I_1\exp(t/\tau_1) + I_2\exp(t/\tau_2) + c$$

The PL lifetimes and their relative contributions to the biexponential fit are shown in Table 2. From these data, we observe that the PL decays faster in the spacerless copolymers **17** than in the corresponding octamethylene-tethered copolymers **18**. The enhanced luminescence quenching in **17** (as evident from the shorter PL lifetime, as well as the lower PL and EL quantum yields) further supports our position. Considering that a significant fraction of the electron−hole recombination occurs at the organometallic center, we propose that the close proximity of the bonded iridium complex to the host polyfluorene in the spacerless copolymers **17** leads to an increase in triplet energy back transfer from the iridium complex to polyfluorene. In contrast, the octamethylene tether in the copolymers **18** offers spatial control of the iridium complex in relation to the conjugated polymer backbone and acts to reduce triplet energy transfer within the system, thereby improving the triplet exciton confinement at the iridium complexes in **18**. In contrast to the room temperature measurements, we observe no difference in the phosphorescence decay between the copolymers **17** and **18** at 20 K (see the Supporting Information). This confirms the temperature activated nature of the energy transfer.

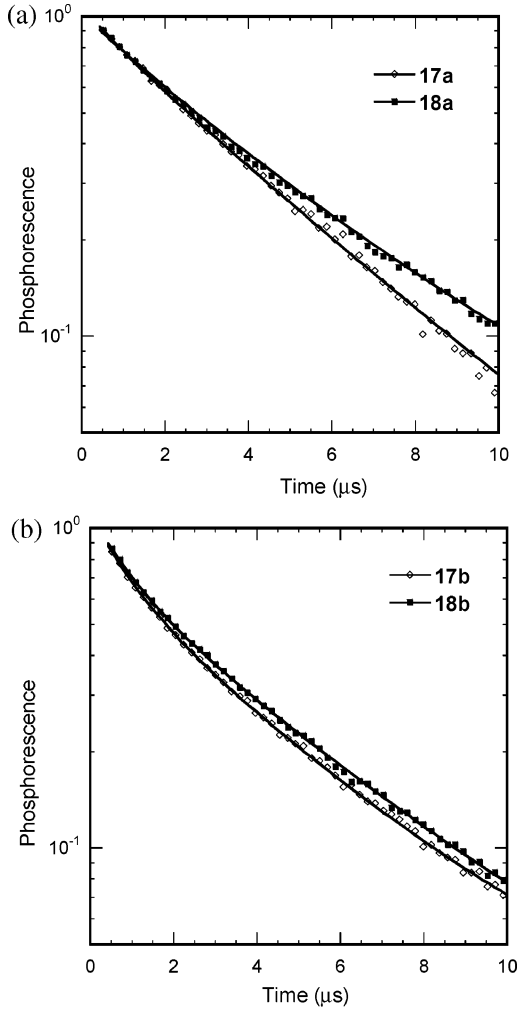

Figure 5. The decay of the photoluminescence intensity (excitation at 355 nm) at room temperature from thin films of (a) the copolymers **17a** and **18a** (lower iridium complex loadings) and (b) the copolymers **17b** and **18b** (higher iridium complex loadings). The solid lines indicate biexponential fits as described in the text.

We note that the increased back transfer in the spacerless copolymers **17** alone cannot fully account for the lower PL quantum yield. We consider the low PL quantum yield of the spacerless copolymer **17** compared with the octamethylene tethered copolymer **18** may be caused by the combination of increased back transfer from guest to host and a lower forward energy transfer from host to guest.

Conclusions

The lower photo- and electroluminescence efficiencies of the spacerless copolymers **17** are consistent with greater Dexter triplet energy transfer in the spacerless systems and with triplet energy back transfer reducing the triplet population at the iridium complexes. We have found that, in thin films, triplet energy back transfer is inhibited in the octamethylene-tethered copolymers **18** by the distance imposed through the tether. We therefore conclude that the incorporation of a spacer between polymer host and phosphorescent guest is an important design principle for achieving higher efficiencies in those electrophosphorescent OLEDs for which the triplet energy levels of the host and guest are similar. Furthermore, we have demonstrated that covalently linking the guest through a tether rather than by conjugative linkage is an important improvement in the design of solution processible electrophosphorescent polymers.

Acknowledgment. We thank the Engineering and Physical Sciences Research Council UK (EPSRC) for financial support and provision of the National Mass Spectrometry Service, Swansea, the Commonwealth Scholarship Commission, Cambridge Commonwealth Trust, Ramsay Memorial Trust (N.R.E.) and the Royal Society (A.K. and S.P.) for financial support. We thank the Australian Research Council, CSIRO, and VESKI for generous support. We thank Dr. A. J. Sandee for numerous discussions and his interest in this work.

Supporting Information Available: General experimental methods, including device fabrication, synthetic procedures, and characterization for **2**−**4**, **6**, **8**−**13**, and **16**−**18**, X-ray diffraction studies and CIF files for **12** and **13** (the data have been deposited in the Cambridge Structural Database: CCDC 276021 and 276022, respectively) and an illustration of the crystal structure of **13**. This material is available free of charge via the Internet at http://pubs.acs.org.

JA0584267